Numerical Solution of Incompressible Flows by a Marching Multigrid Nonlinear Method

Moshe Rosenfeld* and Moshe Israeli†
Technion-Israel Institute of Technology, Haifa, Israel

A downstream marching iterative scheme for the solution of the steady, incompressible, and two-dimensional parabolized or thin layer Navier-Stokes equations is described for a general curvilinear orthogonal coordinate system. Modifications of the primitive equation global relaxation sweep procedure result in an efficient marching scheme. This scheme takes full account of the reduced order of the approximate equations as it behaves like the SLOR method for a single elliptic equation. The proposed algorithm is essentially Reynolds number-independent and therefore can be applied to the solution of the incompressible Euler equations. A judicious choice of a staggered mesh enables second-order accuracy even in the marching direction. The improved smoothing properties permit the introduction of multigrid acceleration. The convergence rates are similar to those obtained by the multigrid solution of a single elliptic equation; the storage is also comparable as only the pressure has to be stored on all levels. Numerical results are presented for several boundary-layer-type flow problems, including the flow over a spheroid at zero incidence.

I. Introduction

CONSIDERABLE evidence has accumulated recently about the applicability of the parabolized Navier-Stokes (PNS) equations for high Reynolds number flows with a principal flow direction (see Rubin[1]). The PNS equations are obtained by neglecting the streamwise viscous terms in the Navier-Stokes equations. When the viscous terms in the circumferential direction are also neglected, one gets the thin layer (TL) approximation.

The steady PNS or TL equations still have an elliptic nature (but of reduced order—see Sec. II) and therefore the initial value problem in the downstream marching direction is not well posed.[2] A well-posed initial-boundary value problem can be formulated by specifying, for example, upstream and side conditions for the velocities and one downstream condition for the pressure. Therefore the PNS equations must be solved globally and cannot be solved by a single-sweep marching.

The reduced order of the PNS equations can be exploited by constructing an iterative marching method for updating the pressure field only.[1] Such a multiple-sweep iteration method has the advantage that the velocity field is generated during the marching process and only the pressure field has to be stored from sweep to sweep—a considerable saving in storage results. However, simple-minded marching does not result in good convergence properties and sometimes diverges. For the two-dimensional case, Israeli and Lin[3,4] devised a stable marching scheme that behaves like the successive line over relaxation (SLOR) method for the solution of a single elliptic equation.

Rubin and Reddy[5] analyzed certain aspects of the solution of the PNS equations and used their procedure to solve several flow problems in Cartesian and axisymmetric body fitted conformal coordinates. They used in most cases a first-order scheme and also applied a simplified one-dimensional multigrid algorithm. Several more recent works are cited in Refs. 6–8.

The present study is a continuation of the work presented in Ref. 9, where the scheme of Israeli and Lin[3,4] was modified into a second-order, staggered, marching multigrid form. The principal aim here is to test the convergence properties of the methods in the case of viscous nonlinear problems and to apply the algorithm to several flow problems. The good smoothing properties of the Israeli and Lin scheme are used in a multigrid framework in order to accelerate the convergence of the solution of the PNS equations. The steady, incompressible, viscous, and two-dimensional equations are considered in a general curvilinear coordinate system. The marching scheme is implemented using a stable algorithm which is second-order accurate also in the marching direction. The same method can be used without modification for the incompressible Euler equations, as the effect of the Reynolds number on the convergence rate is insignificant. In two dimensions, the PNS and the TL equations are identical, and therefore the same analysis applies to both.

II. Formulation

The nondimensional steady, incompressible, and two-dimensional PNS (or TL) equations in a general curvilinear orthogonal coordinate system (ξ, η) are as follows:

Continuity

$$\frac{\partial(h_\xi V)}{\partial \eta} + \frac{\partial(h_\eta U)}{\partial \xi} = 0 \tag{1a}$$

Momentum, η

$$h_\xi \frac{V}{h_\eta}\frac{\partial V}{\partial \eta} + U\frac{\partial V}{\partial \xi} + \frac{UV}{h_\eta}\frac{\partial h_\eta}{\partial \xi} - \frac{U^2}{h_\eta}\frac{\partial h_\xi}{\partial \eta} = -\frac{J}{h_\eta^2}\frac{\partial P}{\partial \eta} + \frac{1}{Re}\frac{\partial}{\partial \eta}\left[\frac{1}{h_\eta^2}\frac{\partial}{\partial \eta}(h_\xi V) - h_\eta U\frac{\partial}{\partial \xi}\left(\frac{1}{h_\eta^2}\right)\right] \tag{1b}$$

Momentum, ξ

$$V\frac{\partial U}{\partial \eta} + h_\eta \frac{U}{h_\xi}\frac{\partial U}{\partial \xi} + \frac{UV}{h_\xi}\frac{\partial h}{\partial \eta} - \frac{V^2}{h_\xi}\frac{\partial h_\eta}{\partial \xi} = -\frac{J}{h^2}\frac{\partial P}{\partial \xi} + \frac{1}{Re}\frac{\partial}{\partial \eta}\left[\frac{1}{J}\frac{\partial}{\partial \eta}(h_\xi U) + h_\eta V\frac{\partial}{\partial \xi}\left(\frac{1}{J}\right)\right] \tag{1c}$$

Presented as Paper 85-1500 at the AIAA Seventh Computational Fluid Dynamics Conference, July 15–17, 1985; received July 18, 1985; revision received Aug. 27, 1986.

*Graduate Student, Department of Aeronautical Engineering; presently, National Research Council Research Associate at NASA Ames Research Center. Member AIAA.

†Professor, Department of Computer Science.

ξ is approximately aligned with the mainstream direction. U and V are the contravariant velocity components in the ξ and η directions respectively. P is the pressure and Re is the Reynolds number. h_ξ and h_η are the Lamme coefficients in the ξ and η directions. J is the Jacobian of the coordinate transformation.

The two-dimensional Navier-Stokes equations are elliptic of order four.[10] It can be shown that the PNS or TL equations are elliptic of order two only—like a single Poisson equation. This ellipticity is caused by the pressure gradient terms via the continuity equation. A well-posed problem can be formulated by defining the boundary conditions as described in Fig. 1 for a rectangular control volume. The following conditions may be specified:

Upstream boundary (AB)

$$U = U_{\text{in}} \qquad V = V_{\text{in}} \tag{2a}$$

Solid wall (AD)

$$U = 0 \qquad V = 0 \tag{2b}$$

Outer boundary (BC)

$$U = U_{\text{out}} \qquad P = P_{\text{out}} \tag{2c}$$

Downstream boundary (CD)

$$\frac{\partial P}{\partial \xi} = \left(\frac{\partial P}{\partial \xi}\right)_{\text{out}} \tag{2d}$$

Other boundary conditions can be used, but the same number of conditions on each boundary must be kept. Subscripts "in" and "out" refer to the inner and outer boundaries, respectively.

III. Discretization

Numerical solutions of Eqs. (1) are obtained by spreading a mesh over the computational domain. Let us assume that the grid points are distributed evenly along the ξ and η coordinates with the spacing Δ and $\Delta\eta$ respectively. When discretizing these equations it should be remembered that their nature should be reflected in the finite-difference approximation.[1,5] In order to be consistent with the boundary-layer (parabolic) nature of the flow, the axial gradients of the velocities should be computed using only upstream values, while the elliptic nature is preserved by forward differencing the axial pressure gradient.[1,5,8] Consequently, it was assumed that a stable marching scheme must be of the first order in the marching direction. But a second-order accuracy can be achieved by a judicious choice of the placement of the variables to be solved at each station. The choice can be explained most easily by considering a Cartesian coordinate system and taking $V = 0$ and $1/Re = 0$ in Eq. (1c), yielding

$$U_\xi^2 = -P_\xi \tag{3}$$

A first-order difference scheme then becomes (see Fig. 2)

$$U_{m,j}^2 - U_{m-1,j}^2 = P_{m,j} - P_{m+1,j} \tag{4}$$

with the unknowns $U_{m,j}$ and $P_{m,j}$. An alternative scheme, first suggested by Israeli[9,11] is written

$$U_{m,j}^2 - U_{m-1,j}^2 = P_{m-1,j} - P_{m,j} \tag{5}$$

with the unknowns $U_{m,j}$ and $P_{m-1,j}$. The scheme is centered about $m + 1/2$ and is of second order.

The same applies to the full viscous PNS or TL equations. At each marching step one solves for all the velocities $U_{m,j}, V_{m,j}$, together with the pressure $P_{m-1,j}$ (for $j = 1, 2, \ldots, J$). Thus, the velocities are indeed solved using values from the upstream while the pressure uses information from the downstream. This approach was subsequently used in Refs. 3 and 8.

In addition, one may stagger the velocity V with respect to the other variables as shown in Fig. 2, where the centering points of the difference equations are also plotted. The differential equations are approximated by central second-order approximations. Whenever needed, averaging was used, as is usually done for staggered grids.

The nonlinear algebraic equations are linearized by either a full Newton-Raphson (NR) method or by performing only one NR iteration. The results are very similar, so usually a single NR iteration is used.

IV. The Multigrid Algorithm

The multigrid technique is a numerical procedure for substantially improving the convergence rate of iterative methods. In order to facilitate comparison with theory, the accommodative C-cycle MG algorithm was chosen.[10] Each MG process consists of three basic parts: relaxation, restriction, and interpolation.

Some of the elements of the present approach were used independently in Ref. 5. Detailed comparisons cannot be made because convergence rates were not presented there. In the present study the MG refinement is applied in both the ξ and η directions, whereas in Ref. 5 the computational mesh was refined only in the streamwise direction (one-dimensional MG procedure).

The Relaxation Scheme

The overall convergence rate of any MG process is strongly influenced by the smoothing properties of the relaxation scheme. It can be shown analytically and experimentally that the usual multiple-sweep marching does not have good con-

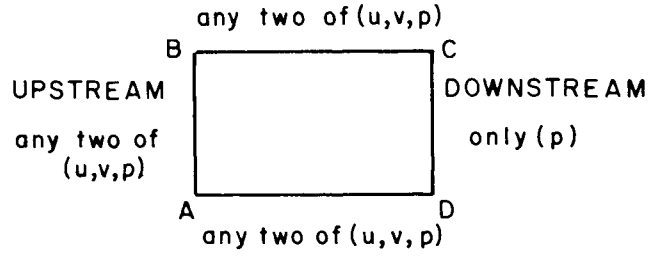

Fig. 1 Example of permissible boundary conditions.

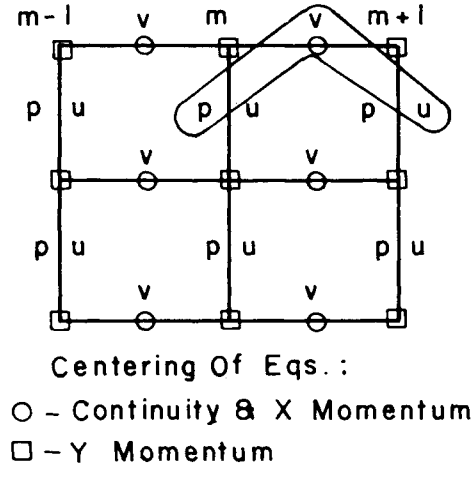

Fig. 2 The staggered grid.

vergence and smoothing properties because short wave errors are not efficiently smoothed. Israeli and Lin[3,4] showed that certain modifications in the streamwise momentum equation which vanish upon convergence give rise to an iterative scheme that is equivalent in the linear case to the SLOR method for a single Poisson equation. In the general nonlinear case, the modified iterative process is essentially equivalent to the relaxation of a single nonlinear Poisson-like equation for the pressure. The velocities can be viewed as auxiliary variables needed during the marching since they have no "memory" by themselves.

Furthermore, the good smoothing properties of the line relaxation scheme of a single Poisson equation were automatically gained. The problems associated with the loss of ellipticity of the difference approximation for the Navier-Stokes equations at high Reynolds number[10] are thus avoided, and no upstream weighting or artificial viscosity is required. There results a considerable saving in storage as well as a simpler relaxation scheme where the convergence rate is essentially independent of the Reynolds number. The same marching algorithm can thus be used for the Euler equation with the same favorable convergence rate.

The extension of the marching scheme of Ref. 4 to a general curvilinear orthogonal coordinate system yields a modified mainstream momentum difference equation (the other difference equations remaining unchanged):

$$-G_m P^*_{m-1} = R_m + \tilde{S}_m \tag{6a}$$

$$P^k_{m-1} = \omega P^*_{m-1} + (1-\omega) P^{k-1}_{m-1} \tag{6b}$$

R_m includes the velocity terms of the finite-difference approximation, m is the marching step number, k is the global iteration index, and ω is the over-relaxation parameter. G_m and $\tilde{S}_m$ are given in Table 1. When the MG procedure is applied, the over-relaxation parameter is $\omega = 1$.

In each marching step, a block tridiagonal system is solved for the vectors U_m, V_m, and P_{m-1}; each component of the vectors corresponds to a point along the η coordinate. Thus, the continuity and the η-momentum difference equations are solved exactly in each step. The streamwise (ξ) momentum equation is not solved exactly since the pressure P_m, taken from the last global iteration, appears in it.

A linear von Neumann stability analysis of the marching iterative scheme for the primitive coupled system of difference equations of Eq. (1) in Cartesian coordinates (Z, Y) was performed by Rubin and Reddy.[5] They numerically determined the eigenvalues of the matrix of the relaxation process and found the estimate $\lambda_{\max} = 1 - C_2(\Delta Z/Y_m)^2$ for $(\Delta Z/Y_m) \gg 1$. Y_m is the outer boundary in the normal Y direction; ΔZ is the interval in the marching direction Z. The rate of convergence is determined by the ratio $\Delta Z/Y_m$. They claim that this conclusion "...differs from that found for the convergence analysis of line relaxation procedures for Poisson solvers. Although the source term S_{ij} leads to the conventional relaxation form of the Laplace operator for the pressure, the coupling with the velocities alters the structure of the inversion matrix and associated spectral radius."

It turns out, however, that the spectral radius $\lambda_{\max}$ can be determined analytically for the coupled PNS system and is independent, in the linear case, of the coupling by the velocities. A stability analysis of the discretized version of Eq. (1) using the modified form Eq. (6) reveals that the amplitude of the errors in the velocities can be related to the error in the pressure field. On the other hand, it was shown[3,4] that in the linearized case the global iteration scheme is reducible to the SLOR method for a single Poisson equation. It follows that all the known results from the theory of the SLOR scheme should be applicable to the present version of the global iterative scheme for the PNS equations. In particular, we find that the maximum eigenvalue $\lambda_{\max}$, which determines the convergence rate, is given in the present case by[12]

$$(\lambda_{\max} + \omega - 1)^2 = \lambda_{\max}\omega^2\mu^2_{\max} \tag{7a}$$

where

$$\mu_{\max} = 1\Big/\left[1 - \left(\frac{\Delta Z}{\Delta Y}\right)^2\left(1 - \cos\pi\frac{\Delta Y}{2Y_m}\right)\right] \tag{7b}$$

for the boundary conditions of Eqs. (2) and with the appropriate scaling. Y_m and ΔY are the outer boundary and the interval in the Y direction respectively. For $\omega = 1$ the maximal eigenvalue is given by

$$\lambda_{\max} \sim 1 - \tfrac{1}{4}(\pi\Delta Z/Y_m)^2 \tag{7c}$$

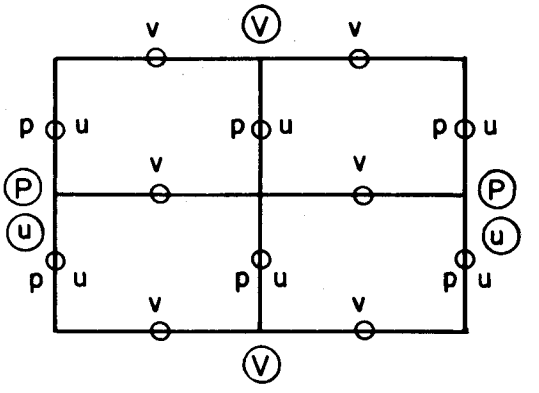

Fig. 3 Relative placement of the variables on two successive MG levels.

Table 1 Definition of G_m and $\tilde{S}_m$

m	G_m	$\tilde{S}_m$
2	$\left(\frac{J}{h_\xi^2}\right)_{m-1/2}$	$-\left(\frac{J}{h_\xi^2}\right)_{m-1/2} P_m$
3	$\left(\frac{J}{h_\xi^2}\right)_{m-3/2} + \left(\frac{J}{h^2}\right)_{m-1/2}$	$-\left(\frac{J}{h_\xi^2}\right)_{m-1/2} P_m - \left(\frac{J}{h_\xi^2}\right)_{m-3/2} (P_{m-1} - P_{m-2} + P^*_{m-1})$
4,5,...	$\left(\frac{J}{h_\xi^2}\right)_{m-3/2} + \left(\frac{J}{h^2}\right)_{m-1/2}$	$-\left(\frac{J}{h_\xi^2}\right)_{m-1/2} P_m - \left(\frac{J}{h_\xi^2}\right)_{m-3/2} P_{m-2} + \left[\left(\frac{J}{h_\xi^2}\right)_{m-3/2} + \left(\frac{J}{h_\xi^2}\right)_{m-5/2}\right] P^*_{m-2} + \tilde{S}_{m-1}$

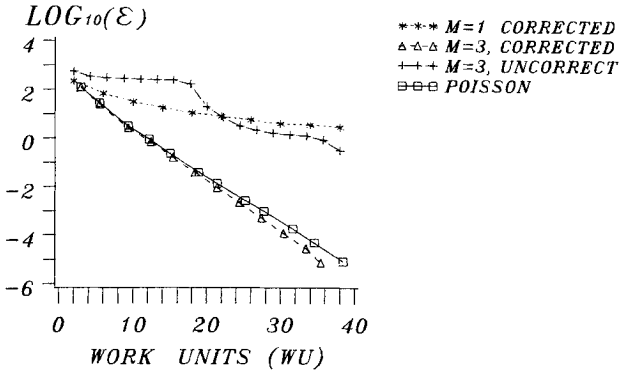

Fig. 4 Convergence history on the finest grid for different relaxation schemes (linear scheme).

Numerical experiments verified the validity of Eq. (7c). For large enough $\Delta Z/Y_m$, the convergence is very rapid and no coarsening of the grid is necessary in the MG procedure. For smaller values of $\Delta Z/Y_m$, the MG procedure is invoked in order to accelerate convergence. For very small values of $\Delta Z/Y_m$ the MG scheme does not seem to be effective, and this indicates that the underlying relaxation scheme breaks down. Since the linear analysis assures convergence for all values of $\Delta Z/Y_m$, it is possible that nonlinear effects, which were neglected in the analysis, adversely affect the convergence rate and the smoothing properties of the relaxation.

Restriction and Storage Requirements

Let the finite-difference approximation of Eqs. (1) on the finest grid M be represented as in Ref. 10:

$$L_j^M \tilde{W}^M(\tilde{x}) = F_j^M(\tilde{x}) \tag{8}$$

where $\tilde{x} = [(\xi, \eta), \tilde{W}^M = U^M, V^M, P^M]^T$ is the exact solution of the difference equations and j is the number of the differential equation ($j = 1,2,3$).

The problem is transferred in the full approximation storage (FAS) mode from the current level k to a coarser level $k-1$ by correcting the right-hand side of Eq. (8) (see Fig. 3):

$$F_j^{k-1}(\tilde{x}) = L_j^{k-1}\left[\tilde{I}_k^{k-1}\tilde{w}^k(\tilde{x})\right] + I_{j,k}^{k-1}\left\{F_j^k(\tilde{x}) - L_j^k\tilde{w}^k(\tilde{x})\right\} \tag{9}$$

$\tilde{w}^k(\tilde{x})$ is an approximation to $\tilde{W}^k(\tilde{x})$. $I_{j,k}^{k-1}$ and $\tilde{I}_k^{k-1}$ are proper restriction operators for the jth equation and for the dependent variables, respectively.

The term within the braces in Eq. (9) is the residual of the jth equation. For the present marching scheme there is no residual in the continuity and in the η-momentum equations since they are solved exactly in each step. The residual of the ξ-momentum equation results only from the streamwise pressure gradient term, and its computation needs only one subtraction. $\tilde{I}_k^{k-1}$ was chosen to be a linear interpolation, which yields $L_1^{k-1}[\tilde{I}_k^{k-1}\tilde{w}^k(\tilde{x})] = 0$ for the continuity equation. $I_{3,k}^{k-1}$ is computed by averaging in both the ξ and η directions. $I_{2,k}^{k-1}$ is a simple injection. In summary, Eq. (9) takes the following form:

$$F_1^{k-1}(\tilde{x}) = 0 \tag{10a}$$

$$F_2^{k-1}(\tilde{x}) = L_2^{k-1}\left[\tilde{I}_k^{k-1}\tilde{w}^k(\tilde{x})\right] \tag{10b}$$

$$F_3^{k-1}(\tilde{x}) = L_3^{k-1}\left[\tilde{I}_k^{k-1}\tilde{w}^k(\tilde{x})\right] + I_{3,k}^{k-1}\left[F_3^k - L_3^k\tilde{w}^k(\tilde{x})\right] \tag{10c}$$

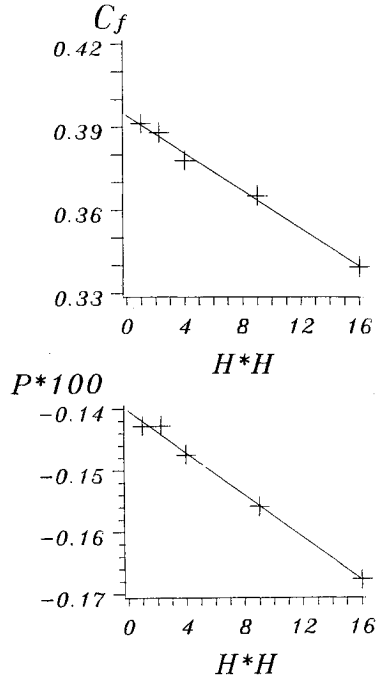

Fig. 5 Accuracy test of the pressure and the normalized skin friction coefficient at $Z = 4$ (semi-infinite flat plate).

Two consequences should be emphasized: 1) only two corrections $[F_2^{k-1}(\tilde{x}), F_3^{k-1}(\tilde{x})]$ have to be computed and stored in the coarse grids, and 2) *all* the dependent variables must be transferred in order to compute the corrections $\{L_j^{k-1}[\tilde{I}_k^{k-1}\tilde{w}^k(\tilde{x})],\ j = 2,3\}$. Since only the pressure is stored, these corrections must be computed during the marching process.

Special attention must be paid to the restriction of the staggered flow variables at the boundaries in order to specify zero corrections as boundary conditions for the coarse grids. In the present study, all the boundary conditions were given at the physical boundaries. The values at the actual staggered placement of each variable at the boundaries were computed by averaging with inner points.

It follows that in addition to the pressure on all grids, one has to save one correction term for each momentum equation on the coarser grids. Assuming N computational points on the finest grid, a simple-minded estimate gives $14N/3$ storage locations for the two-dimensional NS multigrid solution and $2N$ for the PNS marching MG solution.

Interpolation

Since the present marching scheme generates the velocity field from the pressure field, only the correction to the pressure must be interpolated back to the fine grid:

$$P^{k+1} = P^{k+1} + I_k^{k+1}\left(P^k - \tilde{I}_{k+1}^k P^{k+1}\right) \tag{11}$$

I_k^{k+1} is the interpolation operator. In the present case it is a linear operator.

The MG scheme described above is general. But so far only cases in Cartesian coordinate systems with equally spaced grid points were tested with the MG procedure.

V. Results

Linear Case

A linearized version of the PNS equations, expressed in a Cartesian coordinate system, has been tested in Ref. 9. Some of the results are presented here for reference and for comparison with the nonlinear solutions.

Figure 4 compares the convergence history of different relaxation schemes with and without MG acceleration for a

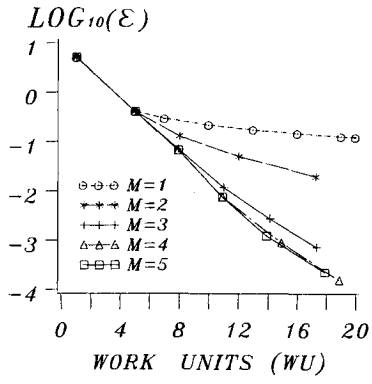

Fig. 6 Convergence history on the finest grid (semi-infinite flat plate).

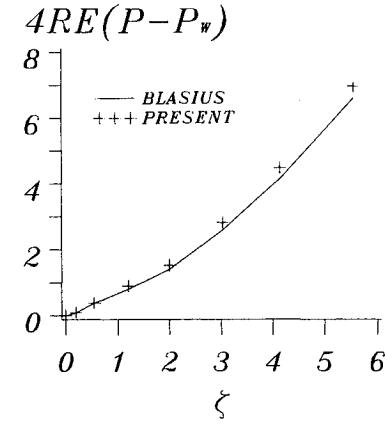

Fig. 7 The pressure profile at $Z = 3$ (semi-infinite flat plate).

finest grid consisting of 17×17 mesh points. The horizontal axis gives the number of work units (WU).[10] A work unit is equivalent to one global iteration on the finest grid. The vertical axis gives the dynamic residual. The MG procedure with three levels ($M = 3$) shows a much better convergence rate than the single grid solution for the same problem. The convergence factor per relaxation iteration (see Ref. 10 for definition) for $M = 3$ is $\hat{\mu} = 0.60$, whereas for the single grid case ($M = 1$) $\hat{\mu} = 0.97$. The linearized PNS equations were also solved without the streamwise correction of Refs. 3 and 4. The MG convergence factor is much worse ($\hat{\mu} = 0.79$). Upon increasing the number of grid points, the unmodified equation's convergence deteriorates. As one can expect, the corrected equations and the solution of the equivalent single Poisson equation for the pressure exhibit very similar convergence properties.

Nonlinear Cases

A series of flow problems were solved with the nonlinear PNS equations. Several test cases were run in a Cartesian coordinate system with possible clustering of mesh points by one-dimensional stretching functions in each direction. Among them we shall mention the flow over an infinite, a semi-infinite, and a finite flat plate, trailing edge flow and an entrance flow between two flat plates. Two cases were run with curvilinear orthogonal coordinate systems: the flow along an axisymmetric cylinder and the flow over a prolate spheroid at zero angle of attack. In the following sections some of the cases will be detailed.

Semi-Infinite Flat Plate

In this case the flow is computed starting from the leading edge, where a uniform velocity $U = 1$, $V = 0$ is given. The downstream boundary was set at $Z = \xi = 4$ and zero pressure gradient was specified there as $\partial P/\partial Z = 0$. On the outer boundary, $U = 1$ and $P = 0$. The no-slip and no-injection conditions were used at the plate.

The second-order accuracy convergence of the finite-difference equations is demonstrated in Fig. 5. The pressure at a fixed point and the normalized skin friction $C_f = C_F\sqrt{Re \cdot Z}$ (which is proportional to the main velocity gradient) at $Z = 4$ are plotted against H^2; H is proportional to the mesh interval.

The convergence history on a finest grid consisting of 65×65 points is shown in Fig. 6 for $Re = 10^3$. The outer boundary is placed at $Y_{max} = 1$ where Y is the normal coordinate ($Y = \eta$). Increasing the number of levels M increases the convergence rate until $M = 4$. The convergence factor per relaxation ($\hat{\mu} = 0.562$) is close to the theoretical value obtained for the solution of a single Poisson equation with the SLOR method ($\hat{\mu} = 0.547$).

For $Re = 10^4$ and $Z = 3$, the pressure distribution as a function of the Blasius similarity coordinate $\zeta = y\sqrt{Re/Z}$ is shown in Fig. 7. The distance from the leading edge is large enough to satisfy the Blasius assumptions; the skin friction coefficient deviates no more than 3% from the theoretical value. The computed pressure is compared with the "Blasius pressure" that can be obtained from the normal momentum equation

$$4ReZ(P - P_w) = f(\zeta f' - f) + 2\zeta f'' \qquad (12)$$

P_w is the pressure on the plate. f is the solution of the Blasius boundary-layer equation for a flat plate with zero pressure gradient. f' and f'' are the first and second derivatives with respect to ζ. The agreement between the present computations and Eq. (12) is good.

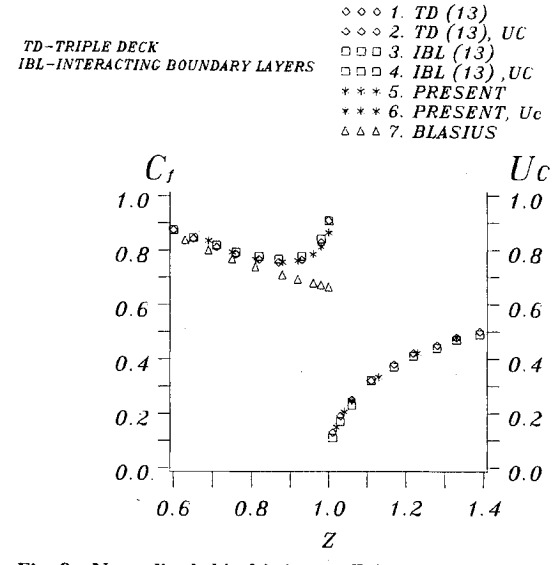

Fig. 8 Normalized skin friction coefficient and wake centerline velocity development (trailing edge flow).

Trailing Edge Flow

The Reynolds number was fixed at $Re = 10^5$ and a grid of 65×73 points was used. The flat plate with zero thickness occupies the interval [0,1] along the $Z(=\zeta)$ axis. We assumed that the interaction is limited to the interval $0.5 < Z < 1.5$. The Blasius solution was specified at the upstream boundary ($Z = 0.5$) and symmetry boundary conditions were given behind the plate. The Blasius solution was approximated by the fourth-order Karman-Pohlhausen velocity profile.

Figure 8 shows the normalized skin friction coefficient ($C_f = C_F\sqrt{Re}$) on the plate ($Z < 1$) and the wake centerline velocity (U_C, $Z > 1$). The agreement with the interacting

boundary layers (IBL) solution and with the triple deck (TD)[13] result is satisfactory.

Entrance Flow Between Two Flat Plates

Uniform inlet conditions were specified at the entrance ($U = 1, V = 0$) while the usual no-slip and no-injection conditions were given at the plates. At the downstream boundary the pressure gradient was calculated by assuming a fully developed flow

$$\frac{\partial P}{\partial Z} = -\frac{12\dot{m}}{Re} \tag{13}$$

$\dot{m}$ is the rate of mass flow.

Figure 9 shows the development of the centerline velocity for two Reynolds numbers, $Re = 20$ and 200, and for a grid of 41×101 points. The results are compared with the full Navier-Stokes computations of Ref. 14. Again the agreement is satisfactory, even at the entrance where the omission of the streamwise diffusion terms may be questionable.

Prolate Spheroid at Zero Angle of Attack

This test case is more stringent because a curvilinear orthogonal prolate spheroid coordinate system is used and the flowfield is more complex than in the previous cases.[15] A nonzero pressure gradient exists at the outer boundary: favorable at the front half and adverse in the rear half. The flowfield eventually separates, with reversed flow near the spheroid. Several numerical solutions of the present problem exist,[15-17] but all of them use the boundary-layer approximation.

The flowfield was computed for a region between the nose and the rear part of the spheroid. The analytically known potential flow is specified at the outer boundary (U and P) and at the downstream boundary ($\partial P/\partial \xi$). At the spheroid the no-slip and no-injection conditions is given. At the upstream boundary the two velocity components are specified. Usually they can be computed from a boundary-layer code. In the present work, the approximate main velocity was computed from a Karman-Pohlhausen profile with a specified skin friction coefficient or displacement thickness. The specified quantity was taken from existing boundary-layer solutions of the same case. The normal component of the velocity V was determined from the potential solution. Numerical experiments show that for reasonable upstream conditions the solution is independent of the upstream conditions, apart from the first few marching steps.

The downstream boundary was set before the separated zone, although the PNS equations are valid there. The computation of flowfields with reversed main flow needs modifications in the approximation of the convection terms.

Two thickness ratios of the axes were considered—4:1 and 6:1. In each case the Reynolds number was $Re = 10^6$ and a single grid consisting of 17×65 points was used (in the η and ξ directions respectively).

Thickness Ratio 4:1

The dependence of the normalized skin friction coefficient ($C_f = C_F\sqrt{Re}$) on the axial distance ($Z = \cos\xi$) is shown in Fig. 10. It compares well with the boundary-layer solution of Ref. 16 but disagrees with Wang's solution.[15]

The point of separation is determined where C_f vanishes. In the present case, the separation point was found to be at

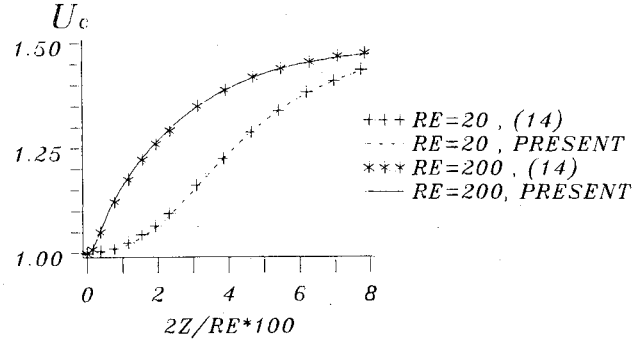

Fig. 9 The development of the centerline velocity (entrance flow).

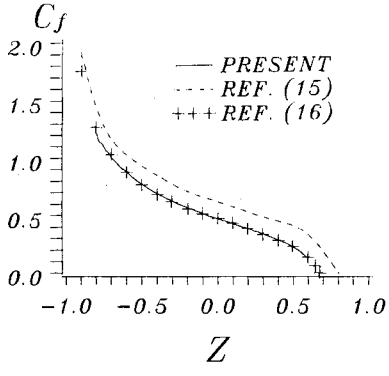

Fig. 10 The distribution of the skin friction coefficient along the spheroid of thickness 4:1.

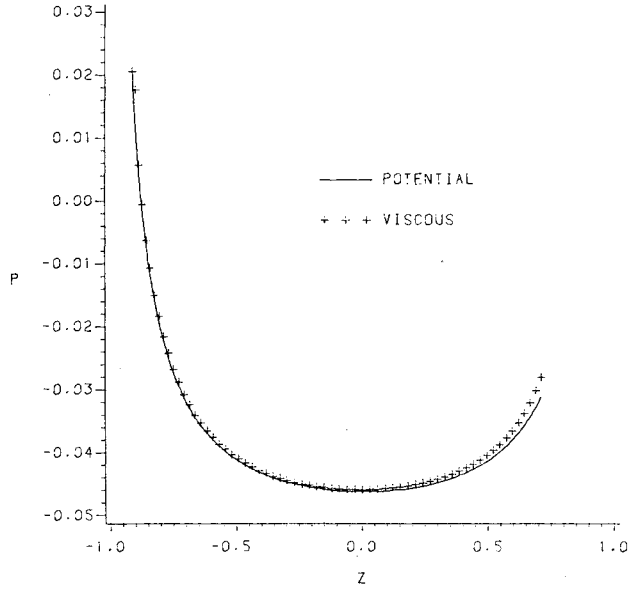

Fig. 11 The pressure distribution along the spheroid of thickness 6:1.

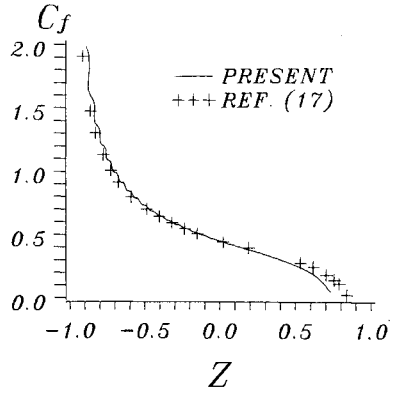

Fig. 12 The distribution of the skin friction coefficient along the spheroid of thickness 6:1.

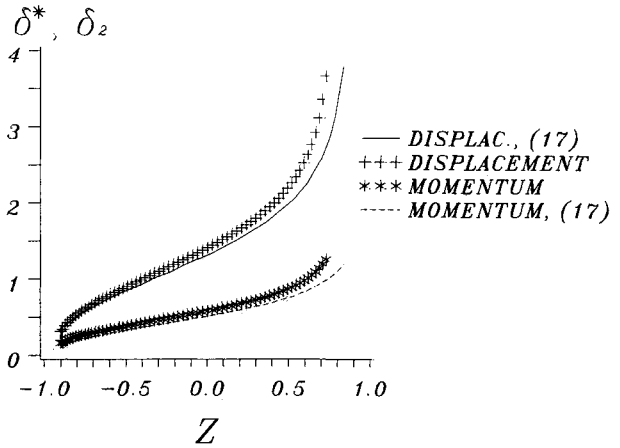

Fig. 13 The development of the integral thicknesses along the spheroid of thickness 6:1.

$Z = 0.67$, which is in excellent agreement with Refs. 16 and 17. Wang[15] has computed the separation point at $Z = 0.84$.

Thickness Ratio 6:1

The pressure distribution on the spheroid, as is found in the PNS solution, is compared with the potential solution in Fig. 11. The agreement is very good except near the downstream boundary. It demonstrates the validity of the boundary-layer approximation for the computation of unseparated flow regions over slender bodies. The slight disagreement near the downstream may be attributed to the improper value being given for the downstream pressure gradient. The potential pressure gradient, as was chosen in this case, is not a good choice near regions of separation.

The skin friction coefficient distribution is compared with a boundary-layer calculation of Schoenauer[17] in Fig. 12. The agreement is good except near the upstream and downstream boundaries. The disagreement in the upstream region probably results from unsatisfactory initial conditions for the velocities. The separation point is found to be closer to the nose ($Z = 0.77$) than in Ref. 17 ($Z = 0.87$), presumably because of the greater adverse pressure gradient computed from the PNS solution. For this more slender body, the separation point is further downstream than in the previous case (with the thickness ratio 4:1).

Figure 13 gives the displacement (δ^*) and the momentum (δ_2) thicknesses dependence on Z. The values computed in the present work are higher than in Ref. 17. The difference is more pronounced near the separation point.

VI. Conclusion

In the present study, an iterative marching method for the solution of the PNS equations is extended to curvilinear orthogonal coordinate systems. Stable second-order-accurate finite-difference equations were developed using central approximation to all derivatives. The solution algorithm is basically equivalent to the solution of a single elliptic equation with the SLOR method. The efficient two-dimensional MG procedure previously developed for a linearized PNS equation was applied to the solution of several nonlinear viscous flows in Cartesian grids. The convergence rates were not adversely affected by the nonlinearity.

Acknowledgment

The second author was partially supported by AFSOR F49620-83-C-0064. The project was supported by Stiftung Volkswagenwerke.

References

[1]Rubin, S.G., "Global Relaxation Procedure for a Reduced Form of the Navier-Stokes Equations," *Proceedings of the Ninth International Conference on Numerical Methods in Fluid Dynamics, Lecture Notes in Physics*, Vol. 218, Springer-Verlag, 1985, pp. 62–71.

[2]Israeli, M., Reitman, V., Salomon, S., and Wolfshtein, M., "On the Marching Solution of the Elliptic Equations in Viscous Fluid Mechanics," *Proceedings of the Second International Conference on Numerical Methods in Laminar and Turbulent Flows*, edited by C. Taylor and B.A. Schrefler, Venice, 1981, pp. 3–14.

[3]Israeli, M. and Lin, A., "Numerical Solution and Boundary Conditions for Boundary Layer Like Flows," *Proceedings of the Eighth International Conference on Numerical Methods in Fluid Dynamics, Lecture Notes in Physics*, Vol. 170, Springer-Verlag, 1982, pp. 266–272.

[4]Israeli, M. and Lin, A., "Iterative Numerical Solutions and Boundary Conditions for the Parabolized Navier-Stokes Equations," *Computers and Fluids*, Vol. 13, No. 4, 1985, pp. 397–409.

[5]Rubin, S.G. and Reddy, D.R., "Analysis of Global Pressure Relaxation for Flows with Strong Interaction and Separation," *Computers and Fluids*, Vol. 11, No. 4, 1983, pp. 281–306.

[6]Khosla, P.K. and Lai, M.T., "Global PNS Solutions for Subsonic Strong Interaction Flow Over a Cone-Cylinder-Boattail Configuration," *Computers and Fluids*, Vol. 11, No. 4, 1983, pp. 325–339.

[7]Khosla, P.K. and Bender, E.E., "Solution of Parabolized Navier-Stokes Equations for Three-Dimensional Internal Flows," *Proceedings of the Ninth International Conference on Numerical Methods in Fluid Dynamics, Lecture Notes in Physics*, Vol. 218, Springer-Verlag, 1985, pp. 296–301.

[8]Reddy, D.R. and Rubin, S.G., "Subsonic/Transonic Viscous/Inviscid Relaxation Procedures for Strong Pressure Interactions," AIAA Paper 84-1627, June 1984.

[9]Israeli, M. and Rosenfeld, M., "Marching Multigrid Solutions to the Parabolized Navier-Stokes (and Thin Layer) Equations," *Proceedings of the Fifth GAMM Conference on Numerical Methods in Fluid Mechanics, Notes on Numerical Fluid Mechanics*, Vol. 7, 1984, pp. 137–144.

[10]Brandt, A. and Dinar, N., "Multigrid Solution to Elliptic Flow Problems," *Numerical Methods for PDE's*, Academic Press, Inc., New York, 1979, pp. 53–147.

[11]Israeli, M., "*Marching Solutions of PNS Equations*," NASA Lewis Seminar, NASA Lewis Research Center, Cleveland, OH, July 1982.

[12]Forsythe, G.E. and Wasow, W.R., "Finite-difference Methods for Partial Differential Equations," Wiley, New York, 1960, pp. 266–271.

[13]Veldman, A.E.P., "New, Quasi-Simultaneous Method to Calculate Interacting Boundary Layers," *AIAA Journal*, Vol. 19, Jan. 1981, pp. 79–85.

[14]Morihara, H. and Cheng, R.T.S., "Numerical Solution of the Viscous Flow in the Entrance Region of Parallel Plates," *Journal of Computational Physics*, Vol. 11, No. 4, 1973, pp. 550–572.

[15]Wang, K.C., "Three-dimensional Boundary Layer Near the Plane of Symmetry of a Spheroid at Incidence," *Journal of Fluid Mechanics*, Vol. 43, Pt. 1, 1970, pp. 187–209.

[16]Hirsh, R.S. and Cebeci, T., "Calculation of Three-Dimensional Boundary Layers with Negative Cross Flow on Bodies of Revolution," AIAA Paper 77-683, June 1977.

[17]Schoenauer, W., private communication, 1985.